PCCP

Accepted Manuscript

ROYAL SOCIETY OF CHEMISTRY

www.rsc.org/pccp

Physical Chemistry Chemical Physics Dynamic Article Links ►

Cite this: DOI: 10.1039/c0xx00000x

www.rsc.org/xxxxxx

ARTICLE TYPE

Unusual electroluminescence from n-ZnO@i-MgO core-shell nanowire color-tunable light-emitting diode at reverse bias

Xiaoming Mo, Guojia Fang,* Hao Long, Songzhan Li, Haoning Wang, Zhao Chen, Huihui Huang, Wei Zeng, Yupeng Zhang, and Chunxu Pan

Light-emitting diodes (LEDs) based on n-ZnO@i-MgO core-shell (CS) nanowires (NWs) were herein demonstrated and characterized. MgO insulating layer was rationally introduced as shells to modify/passivate the surface defects of ZnO NWs. High-quality ZnO/MgO interface was attained and optically pumped near-band-edge emission of the bare ZnO NWs was greatly enhanced after cladding i-MgO shells. Electroluminescence (EL) spectra measured in the whole UV-visible range revealed that light emission can only be detected when LEDs were applied with reverse bias. Moreover, the emission color can be tuned from orange to bright white with increasing reverse bias. We explored these interesting results tentatively in terms of energy-band diagram of the heterojunction and it was found that the interfacial i-MgO shells not only acted as an insulator to prevent short circuit between the two electrodes but also offered a potential energy difference so that electron's tunneling was energetically possible, both of which were essential to generate the reverse-bias EL. The dipole-forbidden d–d transitions by the Laporte selection rule in the p-NiO might be the reason why there is no light being detected from the CS NW LED under forward bias. It is hoped that this simple and facile route may provide an effective approach in designing low-cost CS NW LEDs.

1. Introduction

Nanowire (NW)-based light-emitting diodes (LEDs) have drawn great interest due to their many superior characteristics over the thin-film-based devices.[1-7] The use of NWs offers the ability to grow high quality single crystals, and strains and dislocations are almost non-existent in the NW growth.[8] Nevertheless, due to a large surface-to-volume ratio, surface-defect-related emissions usually play a dominant role in the optical and/or electrical properties of the NW-based optoelectronic devices.[9] These surface defects on the bare NWs can trap the injected carriers which then nonradiatively recombine at the surface or tunnel back to deep-level (DL) centers to produce DL emissions,[10, 11] severely aggravating the performance of the devices. As a result, it is desirable to suppress or eliminate these detrimental surface states if NWs are used as one of the building blocks for high-performance optoelectronic applications. Actually, a core-shell (CS) structure has been developed in the quantum-dot (QD) LEDs to overcome the aforementioned drawback in the past few years and photostability and quantum efficiency of the conventional QDs have been markedly improved by using the CS structures.[12-16] Recently, as inspired by the great achievement of QD LEDs, CS structures were successfully utilized in the NW-based LEDs and laser diodes (LDs),[9, 17] and have been found to be one of the most efficient approaches to improve the performance of NW-based LEDs.

Though there have been many reports on LEDs using CS NW structures up to date, majority of the devices in literature are focused on the performance under forward bias. Since reverse-bias electroluminescence (EL) can function as a useful tool to evaluate the degradation mechanism and reliability of the LED,[18] understanding the reverse-bias EL mechanism of the LED should be very helpful for future high-brightness LED designing. In this work, we have demonstrated an unusual and interesting EL feature from n-ZnO@i-MgO CS NW/p-NiO heterojunction LEDs, in which light emissions can only be detected when the LED is applied with reverse bias. The emission color can also be tuned from orange to bright white with increasing reverse bias. This interesting reverse-bias EL is carefully investigated and related carrier transport and EL mechanisms are proposed and discussed in detail in this study.

2. Experimental

2.1. Fabrication of n-ZnO@i-MgO CS NW/p-NiO LEDs

The schematic structure of the CS NW LEDs is illustrated in Fig. 1a. Firstly, ZnO NWs were grown vertically on the indium tin oxide (ITO)-coated glass substrates (with sheet resistance of 10 ohms per square). A ZnO thin film was produced on the pre-cleaned ITO substrates by decomposing zinc acetate at 400 ^{o}C for 30 min in a tube furnace to provide nucleation sites for vertical ZnO NW growth.[19] ZnO NWs were directly produced on the seeded ITO substrates in transparent glass vials through low-temperature solution method with an aqueous nutrient solution of 25 mM zinc nitrate hexahydrate and hexamethylenetetramine at 80 ^{o}C in an automatic oven. The purpose of selecting glass vials as the reaction containers instead of conventional Teflon-lined autoclaves is to provide a soft and benign NW growth environment, which is beneficial to improve the ZnO crystal qualities.[20] When the reaction was finished, the samples were put into an ultrasonic bath for 5 s to remove the residue, dried under clean nitrogen flow and then rapidly annealed at 550 ^{o}C for 10 min to improve the crystalline qualities of the as-grown NWs.

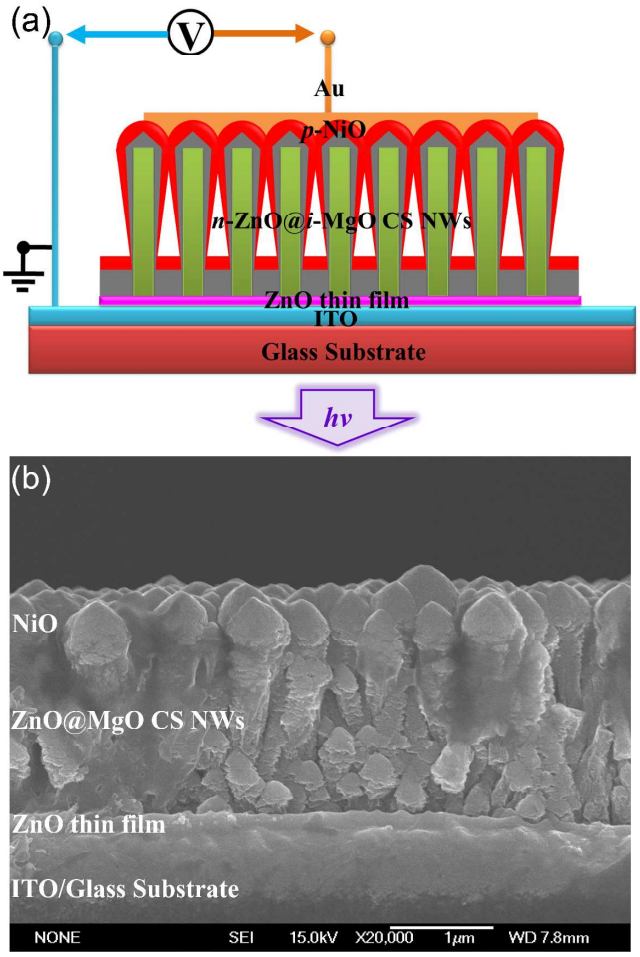

Fig. 1 (a) Schematic structure of the n-ZnO@i-MgO CS NW/p-NiO heterojunction LEDs. (b) Cross-sectional image of n-ZnO@i-MgO CS NW/p-NiO heterojunction.

After annealing, the samples were transferred into a radio frequency (RF) magnetron sputtering chamber immediately to prevent the absorptions of oxygen and moisture. MgO shells were deposited onto the annealed ZnO NWs in the sputtering system at 350 ^{o}C, using an Mg target (99.99% purity) with the Ar and O_2 flow ratio of 1:1. The sputtering power and working pressure were set as 120 W and 1 Pa, respectively. The i-MgO thicknesses were controlled by varying the deposition time to evaluate their impact on the device performance and the optimized deposition time was 20 min. So unless specifically stated otherwise, the article below will apply this optimized condition (average deposition rate of i-MgO was measured to be ~6 nm per min on a referenced quartz substrate). A 400 nm thick p-NiO capping film was then directly sputtered on the CS NWs at 150 ^{o}C to form n-ZnO@i-MgO CS NW/p-NiO heterojunction. An 80 nm Au was sputtered on p-NiO as the anode electrode and ITO was directly used as the cathode. No thermal treatment was carried out before the as-produced LEDs were packaged and characterized.

2.2. Characterization and measurements

Morphology of the as-grown ZnO NWs was characterized by a scanning electron microscopy (SEM, JEOL JSM-6700F). n-ZnO@i-MgO CS NW samples were sonicated in ethanol for 2 h and the suspensions were dropped onto the Cu micro-grids for observation of transmission electron microscope (TEM, JEOL JEM-2010FEF), where high resolution (HR) TEM and energy dispersive X-ray spectrometer (EDS) were performed. The current-voltage (I-V) characteristics were measured by a Keithley 4200 semiconductor parameter analyzer. Hall measurements were conducted via a LakeShore 7704 Hall Measurement System, and it was revealed that the NiO film deposited on a referenced quartz substrate presented p-type conduction with a hole concentration of ~10^{19} cm^{-3} and a resistivity of ~0.2 Ωcm. The optical properties were investigated by PL measurements under a 325 nm He-Cd laser at room temperature (RT) and the emission was collected via a Jobin-Yvon monochromator. The EL spectra were collected by an Acton SpectroPro system coupled with a 2500i monochromator whose grating was set 1800 g/mm blazed at 500 nm for the purpose of detecting the UV-visible emissions. Light emission signals were detected through a photo-multiplier tube (PMT, Princeton Instrument) and the scanning step size was 1 nm. All the EL measurements were carried out at RT.

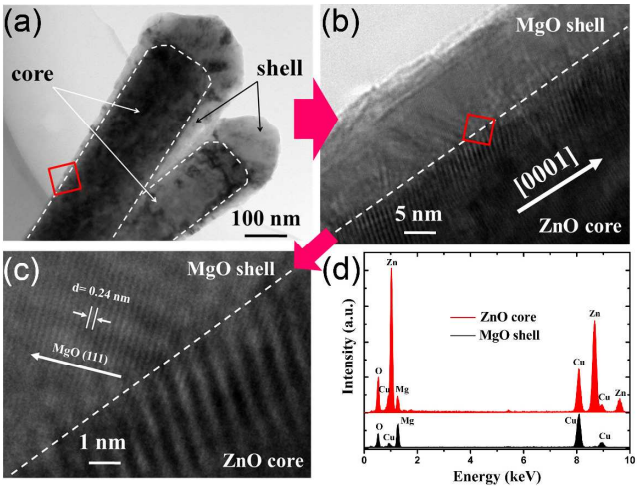

Fig. 2 (a) Typical TEM image of the ZnO NW with i-MgO shell. (b) Zoomed-in image of the red square region in (a). (c) Lattice-resolved HRTEM image of the red square region in (b). (d) EDS spectra measured in the ZnO core side and i-MgO shell side.

3. Results and discussion

Growth time of the as-grown ZnO NWs was optimized to be 16 h to ensure that the interstices between the adjacent ZnO NWs were appropriate for i-MgO shell deposition and further the p-NiO capping, neither too large nor too small. Fig. 1b depicts the typical cross-sectional image of n-ZnO@i-MgO CS NW/p-NiO heterojunction, from which it is observed that the n-ZnO@i-MgO CS NWs are vertically attached on the substrate. Interstices between the adjacent CS NWs are nearly disappeared after p-NiO is deposited and well-defined mushroom-like structures with the heads connected together are attained. From the top view, the p-NiO is covered throughout the whole substrate with many p-NiO grains that are tightly connected with the neighboring grains to form a continuous film (not shown). This morphology is interesting and probably attributed to the strong shadow effect of the neighboring NWs during sputtering.[11] Since gap filling with insulating polymers or photoresists can indeed limit the temperature and heating tolerance of the device, this inorganic p-NiO gap filling is more appropriate to improve the device thermal

stability than the polymers or photoresists.[21]

Further structural characteristics are investigated through TEM measurements. Figs. 2a and 2b show the typical TEM images of the ZnO NW with i-MgO shells. From these images, one can observe that i-MgO is well-cladded on both the top head and the sidewalls of the ZnO NW core with a unique morphology that the cone-like top-head shell thickness is much thicker than the sidewalls due to the shadow effect of the neighboring NWs. Besides, even along the NW core, the shell thickness is not uniform and decreases gradually from top to bottom. From the HRTEM image in Fig. 2c, well-defined ZnO/MgO interface can be observed. No apparent stacking faults can be observed, indicating that i-MgO is of high quality. The d-spacing between the adjacent planes of i-MgO was measured to be ~0.24 nm, revealing that the growth of i-MgO shell is along the (111) direction. The EDS spectra measured at the shell side further confirms that the shell is MgO (black line in Fig. 2d). Besides, Mg is also detected at the ZnO NW core side, suggesting that the NW core is wrapped by i-MgO (red line in Fig. 2d).

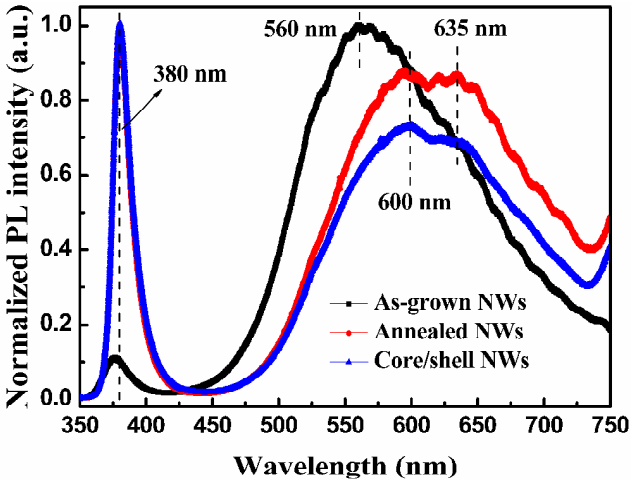

Fig. 3 Normalized PL spectra of as-grown ZnO NWs, ZnO NWs with 550 oC post annealing, and n-ZnO@i-MgO CS NWs.

Fig. 3 presents the normalized PL spectra of as-grown ZnO NWs, ZnO NWs with 550 °C post-annealing, and n-ZnO@i-MgO CS NWs, respectively. According to Fig. 3, all samples demonstrate a ZnO NBE emission from free excitons around 380 nm and a broadband visible DL emission ranging from 450 to 750 nm. The weak NBE emission but predominant DL emission in the as-grown ZnO NWs indicates that there are significant intrinsic defects and surface DL traps in the solution-grown NWs. However, after annealing, the NBE emission of as-grown NWs is increased nearly four times and the visible emission is suppressed, indicative of a great improvement of the ZnO NW crystal quality during annealing. After i-MgO shell cladding, the UV emission intensity can be further increased, making the UV-to-visible ratio increase from 1.1 to 1.5. This result is similar to the previous reports and may be ascribed to the carrier confinement by the ZnO@MgO quantum-well-like structure and the surface modification/passivation by MgO.[9, 11, 17, 22] Furthermore, light extraction can also be improved by the inclusion of MgO shells since the refractive index of MgO (n=1.72) is located between ZnO (n=2.45) and air (n=1.0).[23] It can also be seen that the DL emission center exhibits a redshift from 560 to 600/635 nm, which could be attributed to the transition from oxygen vacancies[24, 25] to oxygen interstitials[26] and/or desorption of OH group[27, 28] during annealing in air.

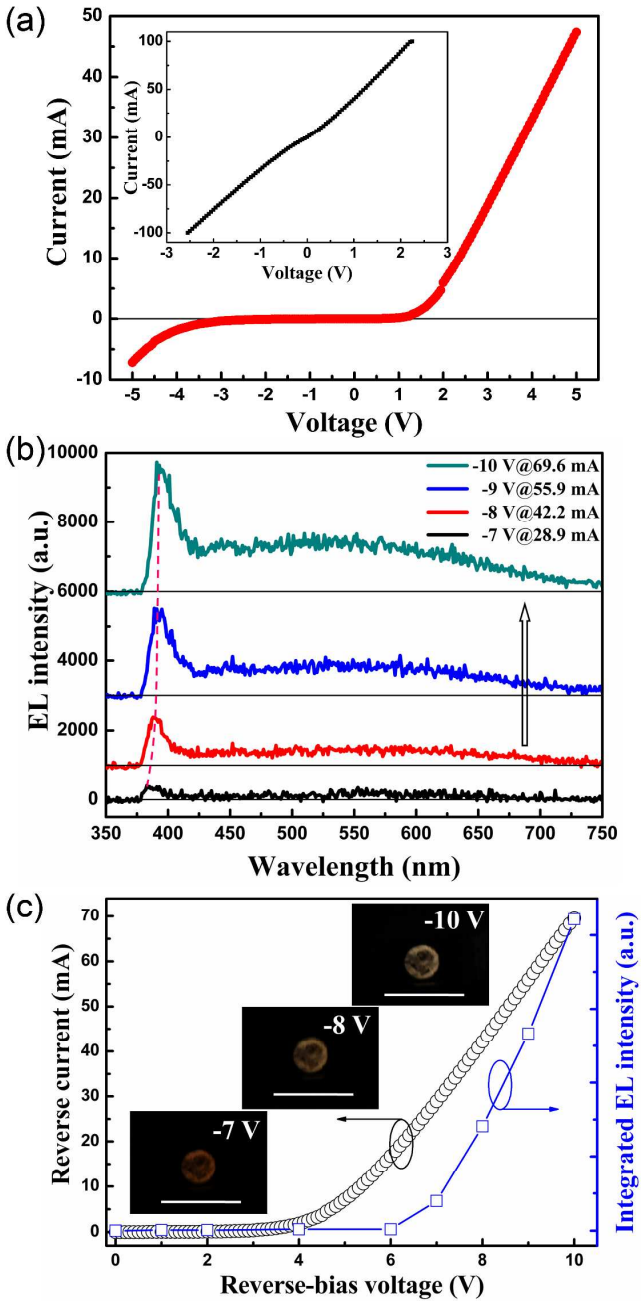

Fig. 4 (a) I-V characteristic of the n-ZnO@i-MgO CS NW/p-NiO heterojunction LED. The inset shows the I-V behavior of the n-ZnO NW/p-NiO device. (b) RT EL spectra of the CS NW LED under reverse biases. (c) Reverse current and integrated EL intensity as a function of the reverse bias. The inset shows the typical emission photographs under reverse biases.

Fig. 4a presents the I-V characteristic of the CS NW LED. The LED demonstrates a rectification property and behaves as a well-defined diode. The flowing current is very small when the reverse bias is below -3 V. With increasing reverse bias, a soft breakdown behavior is observed around -4 V. However, this voltage is still much smaller than the value calculated from 4Eg/q (Eg is the bandgap energy of ZnO or NiO), which means that the

breakdown of the LED is not likely caused by avalanche multiplication but instead might result from the tunneling effect.[29] To confirm the origination of the rectifying characteristic, I-V characteristics from n-ZnO NWs/ZnO thin film/ITO and Au/NiO/Au were measured and plotted (Fig. S1, Supplementary Information). The both ohmic behaviors indicate that no potential barrier heights are existent in the n-ZnO NWs/ZnO thin film/ITO and Au/NiO interfaces. Therefore, it can be confirmed that the rectification characteristic originates from the p-NiO/i-MgO/n-ZnO heterojunctions.

There was also no light being detected from the devices without i-MgO shells either under forward or reverse bias since the I-V behavior of the n-ZnO NW/p-NiO device exhibits like a resistor rather than a diode (see the inset of Fig. 4a). This result suggests that the i-MgO insulation is essential in realizing the EL from the n-ZnO NW/p-NiO LEDs, preventing the short circuit between the two electrodes. In addition, RT EL spectra of the CS NW LEDs were only measured under various reverse biases (with negative voltages applied on p-NiO) because there was no light being detected from all the LED samples in the whole UV-visible range under forward bias (with positive voltages applied on p-NiO) exceeding 13 V.

Fig. 4b shows the RT EL spectra of the CS NW LED under various reverse biases. No light was detected by the EL collecting system unless the reverse bias is above -6 V. At the reverse bias of -7 V, a unique UV emission at around 386 nm starts to emerge, accompanying a DL emission ranging from 450 to 700 nm. The UV emission is not strong enough at such a low bias that it is completely comparable with the DL emission. As the reverse bias is increased from -7 to -10 V, the UV emission increases dramatically and grows quickly dominant, making the UV-to-visible ratio increase from 1.0 to 2.3. As compared with the PL, it is found that the shapes of the EL and PL spectra are very similar regardless of the intensity, especially in the visible range of 450 to 700 nm, indicating that the EL is originated from the ZnO NWs where ZnO NBE and DL (intrinsic defects and surface DL traps) emissions are generated. The EL UV peak, nevertheless, is about 6 to 12 nm to the lower energy as compared with the PL UV peak, which might result from the EL two-stage radiative recombination process where the injected electrons are firstly captured by the shallow surface energy levels in ZnO and then recombine with holes to emit light.[30] In addition, the EL UV peak itself also redshifts to the lower energy from 386 to 392 nm, which can be ascribed to the bandgap variations induced by the heating effect under high injection current.[31, 32]

The emitted light from the LEDs was strong enough to be clearly observed with the naked eyes in a dark room when the reverse bias is above the threshold. The emitting color has been found to be tuned from orange to bright white when the reverse bias increases from -7 to -10 V. The calculated chromaticity coordinates at CIE 1931 are (0.36, 0.39), (0.34, 0.35), (0.31, 0.34) when the reverse bias is -7, -8, and -10 V, respectively, which demonstrates the color change. The corresponding emission photographs illustrated in the inset of Fig. 4c further confirm the feature of color tunability. Since human eyes are not sensitive to the UV light, the observed color change from the LED must be caused by the tunability of visible light that originates from the ZnO DL emission. With increasing reverse bias from -7 to -10 V, more DL defects/traps might be involved in the EL process due to the deformation of equi-potential planes[33] and superposition of these enhanced DL emissions would lead to a gradual change of the emission color from orange to bright white.

The color tunability as well as the feature of light emission only under reverse bias indicates that the EL mechanism and carrier transport of the CS p-i-n heterojunction LEDs in this study might be very different from that of the conventional forward-biased p-n or p-i-n LEDs. Fig. 4c presents the reverse current and integrated EL intensity as a function of the reverse bias. The emission intensity grows rapidly when the bias is above the emission threshold (~-6 V), suggesting that the EL mechanism presumably involves electrons tunneling through the heterojunction.[1] It is also observed that the emission threshold is much larger than the reverse breakdown voltage (~-4 V).

To explicate the EL mechanism, simplified energy-band diagram of the device components referenced to the vacuum level and the energy-band alignment diagram constructed by the Anderson model under forward and reverse bias have been shown in Fig. 5. According to the data from literatures,[2, 23, 34] the p-NiO/n-ZnO heterojunction actually exhibits a type II band alignment and i-MgO acts as an insulating layer that can make a sufficient potential energy difference (see Fig. 5a).

As the device is applied with forward bias (see Fig. 5b), electrons would flow from the n-ZnO conduction band to that of p-NiO by tunnelling through the i-MgO easily because the depletion region and the energy barrier between n-ZnO and i-MgO is weakened by the forward electric field. But for holes, considering that the mobility of holes in the p-NiO is extremely lower than that of the electrons in the n-ZnO, the drift length for holes—$L_p(\varepsilon)=\varepsilon\mu_p\tau_p$, where ε is the electric field, μ_p is the hole mobility, and τ_p is the hole life time—might be much smaller than that of electrons under forward bias. In that case, holes might be very difficult in injecting into ZnO across the depletion region even under high forward bias if an additional blocking of i-MgO is included so that the e-h recombination would dominantly occur in the p-NiO side. Light would not be generated if recombination occurs in p-NiO since d–d transitions in NiO are dipole-forbidden by the Laporte selection rule,[21] which is confirmed by the PL investigation in our study (see Fig. 6). That could be the reason why there is no light being detected from the CS NW LED even under huge forward bias.

However, the situation is completely different when the device is under reverse bias (see Fig. 5c). With increasing reverse bias, the depletion region would be gradually widened and move from i-MgO towards n-ZnO adjacent to the n-ZnO/i-MgO interface. Besides, the electric potential can also gradually lower the n-ZnO conduction band or raises the p-NiO valence band as the reverse bias is increased. In particular, at a specific elevated voltage, electrons in the Au electrode might finally be possible to traverse the barrier between Au and MgO and tunnel into the conduction band of n-ZnO due to the band bending under large electric field at reverse bias, resulting in rapid increase of the reverse current. The consistency between the reverse breakdown

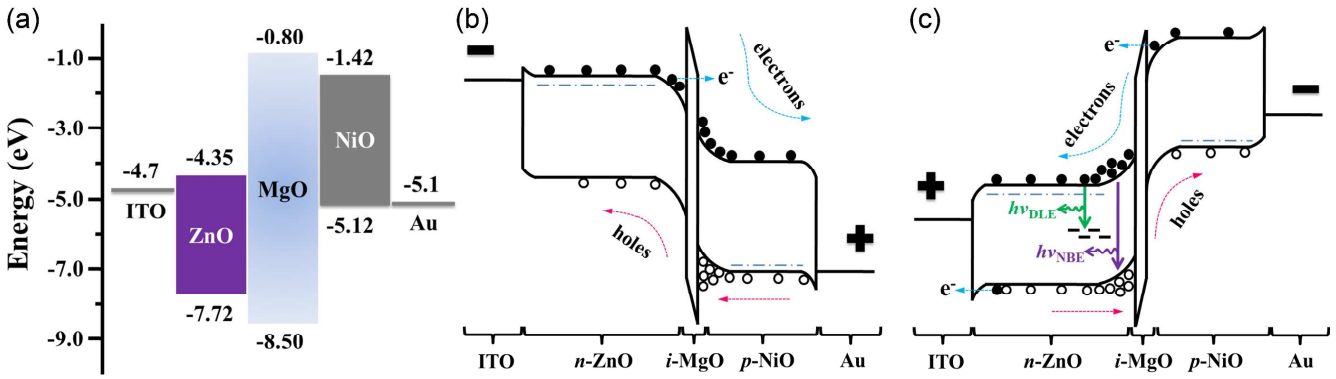

Fig. 5 (a) Simplified energy band diagram of the device components referenced to the vacuum level. (b) and (c) present the energy-band alignment diagram of the n-ZnO@i-MgO CS NW/p-NiO heterojunction under forward and reverse bias, respectively.

voltage (~-4 V) and the energy barrier between Au and MgO (~4.3 eV) confirms the discussion above.

On the other hand, the ITO Fermi level could also gradually traverse the ZnO bandgap with increasing reverse bias. As a result, numerous electrons trapped in the DLs in ZnO can then tunnel into the ITO electrode under sufficient reverse bias, leaving behind holes in the DLs which can recombine radiatively with the conduction band electrons to emit DL emission. If the reverse bias is high enough, the n-ZnO valence band electrons could tunnel into the ITO electrode as well, which is equivalent to hole back-injection into ZnO.[35, 36] The injected holes can be driven to the depletion region adjacent to the n-ZnO/i-MgO interface and radiatively recombine with the conduction band electrons, generating the dominant UV emission via the band-to-band transition or the broadband DL emission through the intrinsic defects and surface DL traps.

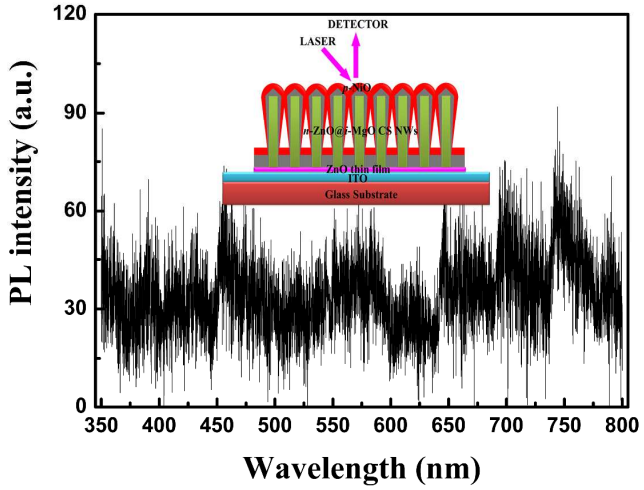

Fig. 6 PL spectrum of n-ZnO@i-MgO CS NW/p-NiO heterojunction, where the incident 325 nm He-Cd laser is penetrated from the p-NiO.

Note that the injected holes might not be sufficient enough to recombine with the tunneling electrons to emit detectable light under low reverse-bias voltages. That is why much higher emission threshold voltage is needed to light up the device as compared with the breakdown voltage (see Fig. 4c). In addition, some previous reports also proposed that electron-hole pairs could be generated in the insulating layer through impact ionization.[37-39] This effect might work at high bias-voltages and should be considered.

It is worth noting that tens of LED samples have been prepared and characterized after observing this interesting EL characteristic. Similar emission behavior only under reverse bias can be observed from all the LED samples, confirming that this behavior is not accidental. Actually, light emission under both forward and reverse bias has been previously observed in many n-ZnO/p-GaN[40-43], n-ZnO/p-Si[44] and n-GaN/Si[35, 36] LEDs. However, articles about lighting up only under reverse bias are very rare.[1, 29] In the LEDs of lighting up only under reverse bias, it has been suggested that the tunneling electrons from the p-GaN valence band to the n-ZnO conduction band or to the DL states near the n-ZnO/p-GaN interface are responsible for the reverse current. For the situation in our LEDs, however, these tunnelling regimes might be deeply suppressed due to the blocking of i-MgO shells. Therefore, the leakage current at low applied voltage might derive from shunt tunneling of electrons through the intrinsic defects of i-MgO shells. In addition, it is interesting that no light can be detected either under forward or reverse bias without i-MgO in our study. In fact, i-MgO shells not only provide good insulation to prevent short circuit between the electrodes, but also offer a potential energy difference so that electron's tunneling is energetically possible, both of which are essential to generate the reverse-bias EL.

4. Conclusions

In summary, we demonstrated an unusual and interesting EL emission from n-ZnO@i-MgO CS NW/p-NiO heterojunction LEDs using MgO insulator as the shells to modify/passivate the surface defects of ZnO NWs. The NBE emission of bare ZnO NWs was greatly enhanced with cladding i-MgO shells whereas the DL emission was suppressed. EL spectra measured in the whole UV-visible range revealed that light emissions can be detected only under reverse bias. The emission color can also be tuned from orange to bright white when the reverse bias was increased. Related carrier transport and EL mechanisms were investigated in terms of energy-band diagram. It was found that i-MgO not only provided good insulation for preventing short circuit between the electrodes, but also offered a potential energy difference so that electron's tunneling was energetically possible, both of which were essential to generate the reverse-bias EL. The dipole-forbidden d–d transitions by the Laporte selection rule in

the p-NiO might be the reason why there is no light being detected from the CS NW LED even under huge forward bias. It is hoped that this simple and facile route may provide an effective approach in designing low-cost CS NW LEDs.

Acknowledgements

This work was supported by the 973 Program (2011CB933300) of China, the National Natural Science Foundation of China (61376013, J1210061), the Research Program of Wuhan Science & Technology Bureau (2013010501010141), the Natural Science Foundation of Jiangsu Province (BK20131186), and the Shenzhen Strategic Emerging Industry Development Funds (JCYJ20130401160028796).

Notes and references

School of Physics and Technology, Key Lab of Artificial Micro- and Nano-Structures of Ministry of Education, Wuhan University, Wuhan 430072, People's Republic of China. Fax: +86 (0)27 68752569; Tel: +86 (0)27 68752147; E-mail: gjfang@whu.edu.cn.

†Electronic Supplementary Information (ESI) available:

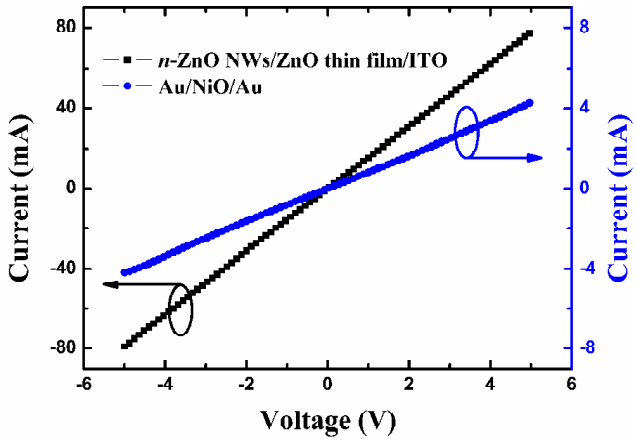

Fig. S1 I-V curves of n-ZnO NWs/ZnO thin film/ITO and Au/NiO/Au. The both ohmic behaviors indicate that no potential barrier heights are existent in the n-ZnO NWs/ZnO thin film/ITO and Au/NiO interfaces. Therefore, it is confirmed that the rectification characteristic originates from the p-NiO/i-MgO/n-ZnO heterojunctions.

1. G. C. Yi and W. I. Park, *Adv. Mater.*, 2004, **16**, 87-90.
2. O. Lupan, T. Pauporté and B. Viana, *Adv. Mater.*, 2010, **22**, 3298-3302.
3. S. Xu, C. Xu, Y. Liu, Y. Hu, R. Yang, Q. Yang, J. H. Ryou, H. J. Kim, Z. Lochner, S. Choi, R. Dupuis and Z. L. Wang, *Adv. Mater.*, 2010, **22**, 4749-4753.
4. Y. S. Choi, J. W. Kang, D. K. Hwang and S. J. Park, *IEEE Trans. Electron Devices,* 2010, **57**, 26-41.
5. X. W. Sun, J. Z. Huang, J. X. Wang and Z. Xu, *Nano Lett.*, 2008, **8**, 1219-1223.
6. X. M. Zhang, M. Y. Lu, Y. Zhang, L. J. Chen and Z. L. Wang, *Adv. Mater.*, 2009, **21**, 2767-2770.
7. F. Fang, D. Zhao, B. Li, Z. Zhang and D. Shen, *Phys. Chem. Chem. Phys.*, 2010, **12**, 6759-6762.
8. A. Sanders, P. Blanchard, K. Bertness, M. Brubaker, C. Dodson, T. Harvey, A. Herrero, D. Rourke, J. Schlager and N. Sanford, *Nanotechnology*, 2011, **22**, 465703.
9. C. Y. Lee, J. Y. Wang, Y. Chou, M. Y. Liu, W. F. Su, Y. F. Chen and C. F. Lin, *J. Appl. Phys.*, 2010, **107**, 034310.
10. A. van Dijken, E. A. Meulenkamp, D. Vanmaekelbergh and A. Meijerink, *J. Phys. Chem. B*, 2000, **104**, 1715-1723.
11. W. Liu, Y. Liang, H. Xu, L. Wang, X. Zhang, Y. Liu and S. Hark, *J. Phys. Chem. C*, 2010, **114**, 16148-16152.
12. K. S. Cho, E. K. Lee, W. J. Joo, E. Jang, T. H. Kim, S. J. Lee, S. J. Kwon, J. Y. Han, B.-K. Kim, B. L. Choi and J. M. Kim, *Nat. Photonics*, 2009, **3**, 341-345.
13. E. Jang, S. Jun, H. Jang, J. Lim, B. Kim and Y. Kim, *Adv. Mater.*, 2010, **22**, 3076-3080.
14. K. W. Song, R. Costi and V. Bulović, *Adv. Mater.*, 2013, **25**, 1420-1423.
15. Y. Shirasaki, G. J. Supran, M. G. Bawendi and V. Bulović, *Nat. Photonics*, 2012, **7**, 13-23.
16. E. M. Likovich, R. Jaramillo, K. J. Russell, S. Ramanathan and V. Narayanamurti, *Adv. Mater.*, 2011, **23**, 4521-4525.
17. C. Y. Liu, H. Y. Xu, J. G. Ma, X. H. Li, X. T. Zhang, Y. C. Liu and R. Mu, *Appl. Phys. Lett.*, 2011, **99**, 063115.
18. H. Chen, *Appl. Phys. Lett.*, 2013, **102**, 162106-162103.
19. L. E. Greene, M. Law, D. H. Tan, M. Montano, J. Goldberger, G. Somorjai and P. Yang, *Nano Lett.*, 2005, **5**, 1231-1236.
20. B. Q. Cao, W. P. Cai, Y. Li, F. Q. Sun and L. D. Zhang, *Nanotechnology*, 2005, **16**, 1734-1738.
21. B. O. Jung, Y. H. Kwon, D. J. Seo, D. S. Lee and H. K. Cho, *J. Cryst. Growth*, 2013, **370**, 314-318.
22. J. P. Richters, T. Voss, D. S. Kim, R. Scholz and M. Zacharias, *Nanotechnology*, 2008, **19**, 305202.
23. H. Zhu, C. X. Shan, J. Y. Zhang, Z. Z. Zhang, B. H. Li, D. X. Zhao, B. Yao, D. Z. Shen, X. W. Fan, Z. K. Tang, X. Hou and K. L. Choy, *Adv. Mater.*, 2010, **22**, 1877-1881.
24. P. Yang, H. Yan, S. Mao, R. Russo, J. Johnson, R. Saykally, N. Morris, J. Pham, R. He and H. J. Choi, *Adv. Funct. Mater.*, 2002, **12**, 323-331.
25. K. Vanheusden, C. H. Seager, W. L. Warren, D. R. Tallant and J. A. Voigt, *Appl. Phys. Lett.*, 1996, **68**, 403.
26. E. Lai, W. Kim and P. Yang, *Nano Res.*, 2008, **1**, 123-128.
27. S. Kishwar, K. ul Hasan, N. H. Alvi, P. Klason, O. Nur and M. Willander, *Superlattices Microstruct.*, 2011, **49**, 32-42.
28. K. Tam, C. Cheung, Y. Leung, A. Djurišic, C. Ling, C. Beling, S. Fung, W. Kwok, W. Chan and D. Phillips, *J. Phys. Chem. B*, 2006, **110**, 20865-20871.
29. H. Chen, M. Chen, Y. Huang, W. Sun, W. Li, J. Yang, H. Kuan and M. Shiojiri, *IEEE Trans. Electron Devices*, 2011, **58**, 3970-3975.
30. E. S. M. Goh, H. Y. Yang, Z. J. Han, T. P. Chen and K. Ostrikov, *Appl. Phys. Lett.*, 2012, **101**, 263506.
31. S. Chu, M. Olmedo, Z. Yang, J. Kong and J. Liu, *Appl. Phys. Lett.*, 2008, **93**, 181106.
32. H. H. Huang, G. J. Fang, X. M. Mo, H. Long, L. Yuan, B. Z. Dong, X. Q. Meng and X. Z. Zhao, *IEEE Electron Device Lett.*, 2009, **30**, 1063-1065.
33. Y. J. Hong, C. H. Lee, A. Yoon, M. Kim, H. K. Seong, H. J. Chung, C. Sone, Y. J. Park and G. C. Yi, *Adv. Mater.*, 2011, **23**, 3284-3288.
34. R. Deng, B. Yao, Y. F. Li, Y. M. Zhao, B. H. Li, C. X. Shan, Z. Z. Zhang, D. X. Zhao, J. Y. Zhang, D. Z. Shen and X. W. Fan, *Appl. Phys. Lett.*, 2009, **94**, 022108.
35. A. Z. Mariano, B. Jiming, S. Ilan, Y. Wei, Y. Joonah, N. Venkatesh and C. Federico, *Nanotechnology*, 2007, **18**, 235205.
36. A. Z. Mariano, B. Jiming, S. Ilan, Y. Wei, N. Venkatesh and C. Federico, *Nanotechnology*, 2007, **18**, 395201.
37. P. L. Chen, X. Y. Ma and D. R. Yang, *Appl. Phys. Lett.*, 2006, **89**, 111112.
38. H. Zhu, C. X. Shan, B. H. Li, Z. Zhang, D. Z. Shen and K. L. Choy, *J. Mater. Chem.* 2011, **21**, 2848-2851.
39. S. Z. Li, G. J. Fang, H. Long, X. M. Mo, H. H. Huang, B. Z. Dong and X. Z. Zhao, *Appl. Phys. Lett.*, 2010, **96**, 201111.
40. X. Chen, A. Ng, F. Fang, A. Djurišić, W. Chan, H. Tam, K. Cheah, P. Fong, H. Lui and C. Surya, *J. Electrochem. Soc.*, 2010, **157**, H308-H311.
41. X. Chen, A. M. C. Ng, F. Fang, Y. H. Ng, A. B. Djurišic, H. L. Tam, K. W. Cheah, S. Gwo, W. K. Chan and P. W. K. Fong, *J. Appl. Phys.*, 2011, **110**, 094513.

42. M. K. Wu, Y. T. Shih, W. C. Li, H. C. Chen, M. J. Chen, H. Kuan, J. R. Yang and M. Shiojiri, *IEEE Photonics Technol. Lett.*, 2008, **20**, 1772-1774.
43. J. Sadaf, M. Israr, S. Kishwar, O. Nur and M. Willander, *Semicond. Sci. Tech.*, 2011, **26**, 075003.
44. J. Bao, M. A. Zimmler, F. Capasso, X. Wang and Z. F. Ren, *Nano Lett.*, 2006, **6**, 1719-1722.